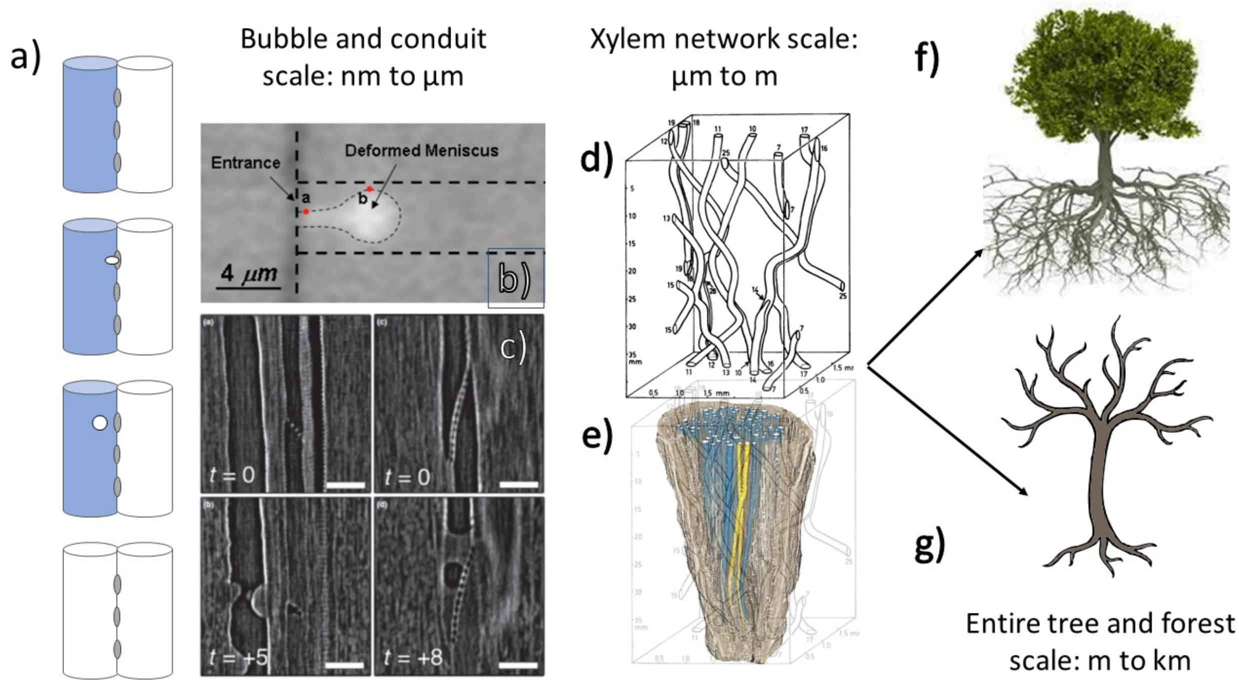

Figure 1. Scales of hydraulic phenomena in woody plants addressed in this review; a) air-seeding of xylem conduits resulting in embolism spread, blue = water-filled, functional conduit, white = air-filled, non-functional conduit, moving from top to bottom is increasing xylem tension (adapted from Zimmermann, 1983); b) Visual observation of air-seeding in a synthetic nanofluidic channel, from Duan et al., 2012; c) refilling of an embolized vessel in grapevine, from Brodersen et al., 2018; d) early work on vessel networks from Zimmermann & Brown, 1971; more recent work showing vessel network properties, yellow vessels are connected, blue vessels are unconnected, from Johnson et al., 2014; f) live tree indicating a functional hydraulic transport system; g) when hydraulic transport fails the result is tree death. All images reproduced with permission.

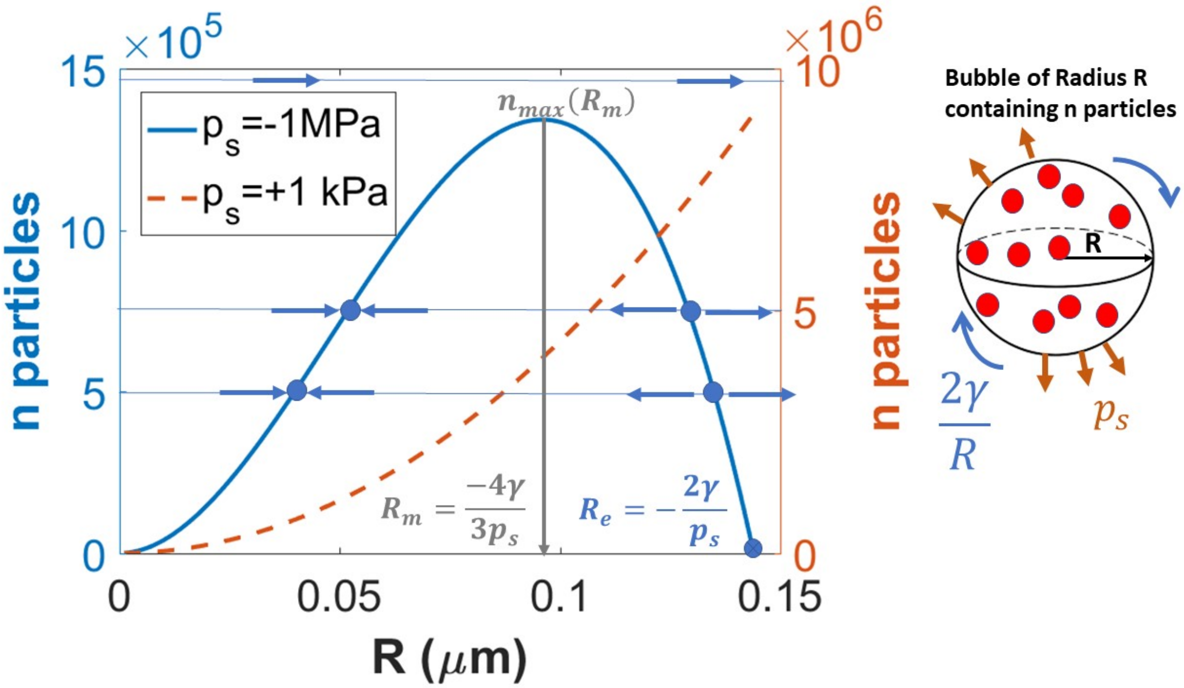

Figure 2: Analysis of bubble stability represented by the number of molecules (n_i) as a function of bubble radius ($\underline{R}$) that can be accommodated under two extremes of xylem pressures (p_s) using the formulation in Konrad & Roth-Nebelsick (2003). When $n_i < n_{max}$ and $R < R_e$, the bubble remains stable and harmless to the xylem. When $n_i < n_{max}$ and $R > R_e$, the bubble will grow and may burst. When $n_i > n_{max}$, the bubble will rapidly grow and likely burst. When $p_s > 0$, there is no catastrophe. When $p_s < 0$, the catastrophe is of a 'fold' type with one stable or attractive branch and one repelling or unstable branch. The critical point defining the fold catastrophe is the point (R_m, n_{max}).

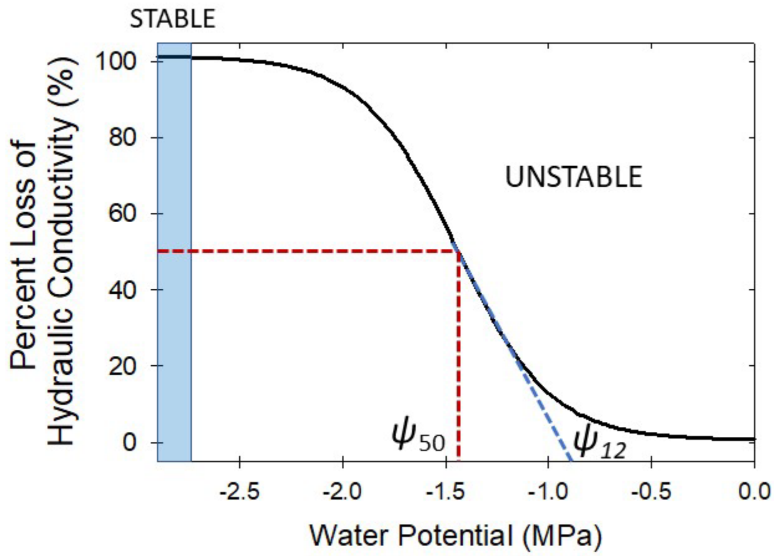

Figure 3. A typical xylem vulnerability curve (VC) as a function of xylem tension (water potential). The PLC=0% is an 'unstable equilibrium' whereas infinite xylem tension leads to a stable equilibrium at PLC=100%. ψ_{50} and ψ_{12} are the xylem tensions and 50 and 12 per cent loss of conductivity, respectively. At least one vessel member must be embolized to initiate small deviations from the zero-water potential state.

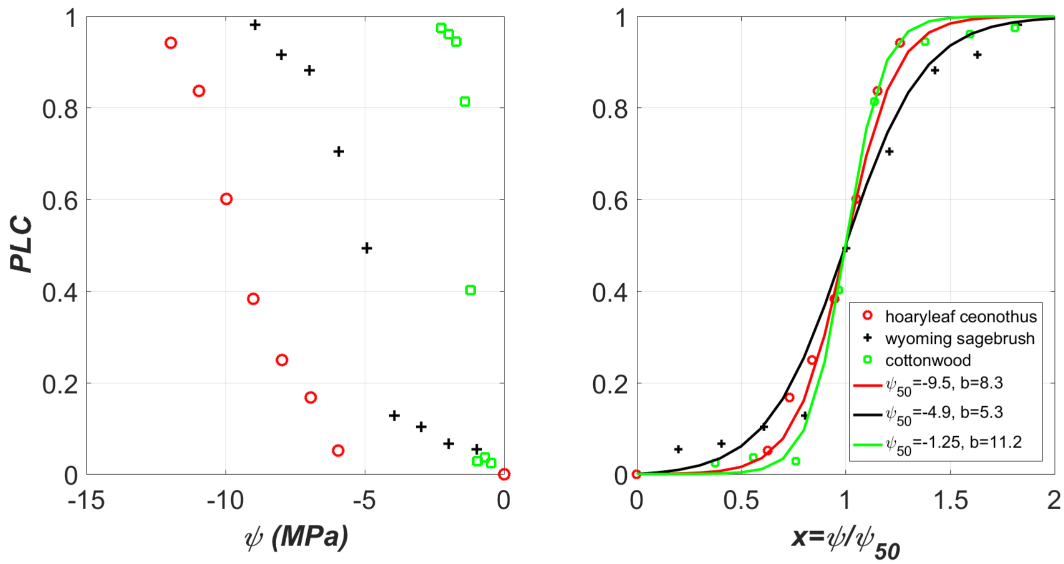

Figure 4: Left: Variations of measured xylem vulnerability curves (VC) across 3 species ranging from desert shrubs to riparian trees (data digitized by us from Sperry, 2000). Right: The *PLC* variations for normalized xylem pressure ($x = \psi/\psi_{50}$) along with the logistic fit to them yielding the ease of cavitation spread parameter b. Note the approximate 'collapse' of the VCs with x on a single curve and that the remaining shape differences can be explained by b.

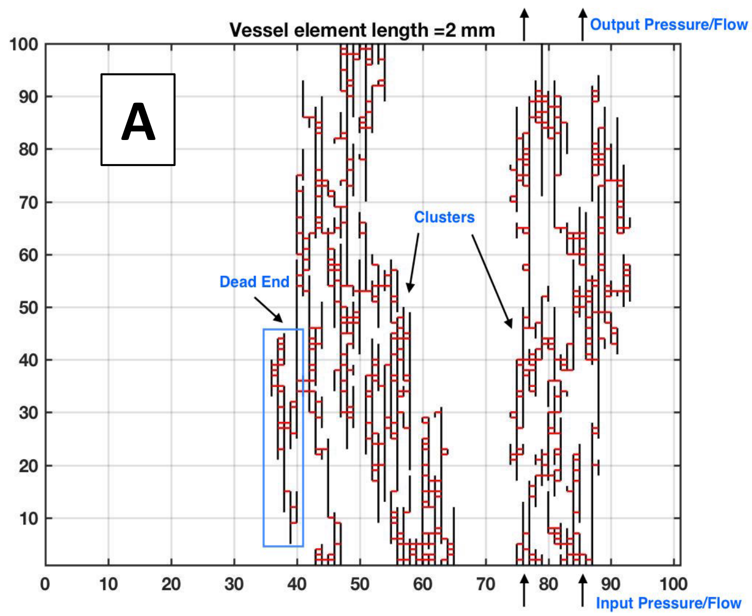

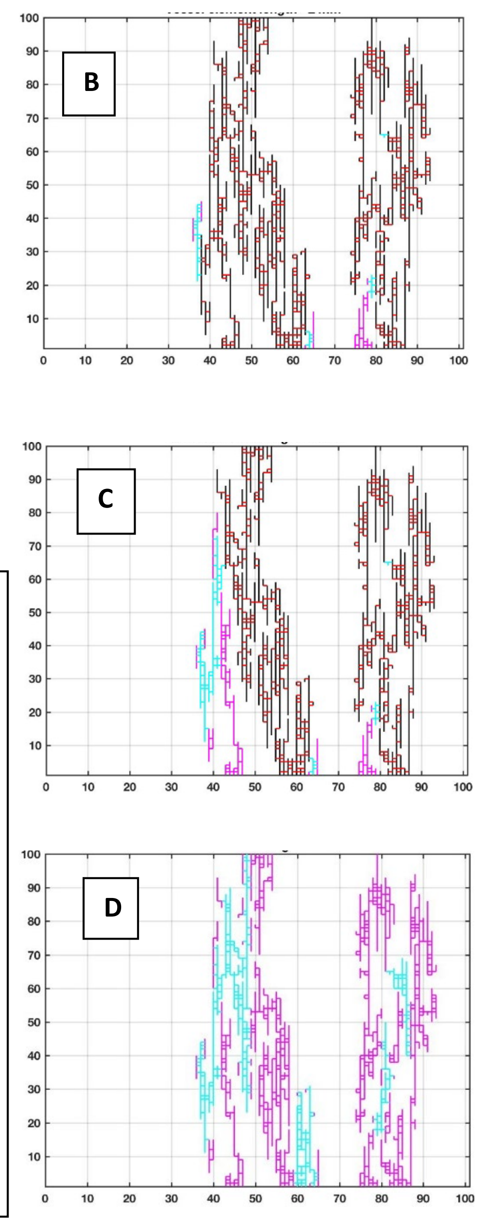

Figure 5: A) Xylem model network on a 100 x 100 grid. Vertical (black) lines correspond to vessels made up of stacked vessel elements. In this case, the xylem segment is 200 mm long. Horizontal (red) lines correspond to pit membranes (simple pits in the case of angiosperms). For easier visualization of the pit membranes that have negligible thickness compared to vessel lengths, horizontal grid lines are not to scale. Some vessels conduct more xylem water than others do and in this example, the ones located in the "dead end" as represented above conduct a relatively negligible amount of water. Simulation of an air injection experiment with 2 initial random embolisms in each cluster (blue) leaving other vessels isolated (magenta) is represented in B). As air pressure is increased incrementally, initial embolisms propagate and 9 embolized vessels (as opposed to 4 in B) are visible in C. Simulations continues until both clusters becomes completely disconnected and non-conducting (D).

Figure 5: A) Xylem model network on a 100 x 100 grid. Vertical (black) lines correspond to vessels made up of stacked vessel elements. In this case, the xylem segment is 200 mm long. Horizontal (red) lines correspond to pit membranes (simple pits in the case of angiosperms). For easier visualization of the pit membranes that have negligible thickness compared to vessel lengths, horizontal grid lines are not to scale. Some vessels conduct more xylem water than others do and in this example, the ones located in the "dead end" as represented above conduct a relatively negligible amount of water. Simulation of an air injection experiment with 2 initial random embolisms in each cluster (blue) leaving other vessels isolated (magenta) is represented in B). As air pressure is increased incrementally, initial embolisms propagate and 9 embolized vessels (as opposed to 4 in B) are visible in C. Simulations continues until both clusters becomes completely disconnected and non-conducting (D).

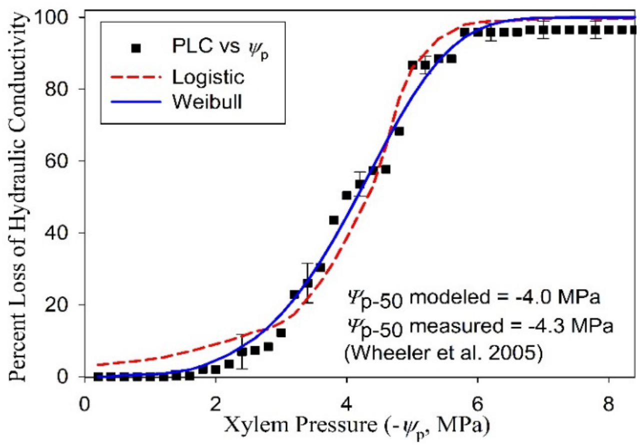

Figure 6 – The VC of the xylem network earlier shown (filled squares) as percent loss in hydraulic conductivity against xylem tension. To eliminate the effect of random initial embolism locations, 40 air-injection simulations were performed and averaged. Logistic and Weibull fits to VCs are shown for reference. Vertical bars represent variability corresponding to initial condition sensitivity. No statistically significant difference between logistic and Weibull were apparent in this case though the Weibull shape better captures the simulation outcome at low xylem pressures . The estimated xylem pressure at which ψ_{P50} occurred are also compared well with measured ψ_{P50} in a similar network (Wheeler et al., 2005)

Figure 6 – The VC of the xylem network earlier shown (filled squares) as percent loss in hydraulic conductivity against xylem tension. To eliminate the effect of random initial embolism locations, 40 air-injection simulations were performed and averaged. Logistic and Weibull fits to VCs are shown for reference. Vertical bars represent variability corresponding to initial condition sensitivity. No statistically significant difference between logistic and Weibull were apparent in this case though the Weibull shape better captures the simulation outcome at low xylem pressures . The estimated xylem pressure at which ψ_{P50} occurred are also compared well with measured ψ_{P50} in a similar network (Wheeler et al., 2005)

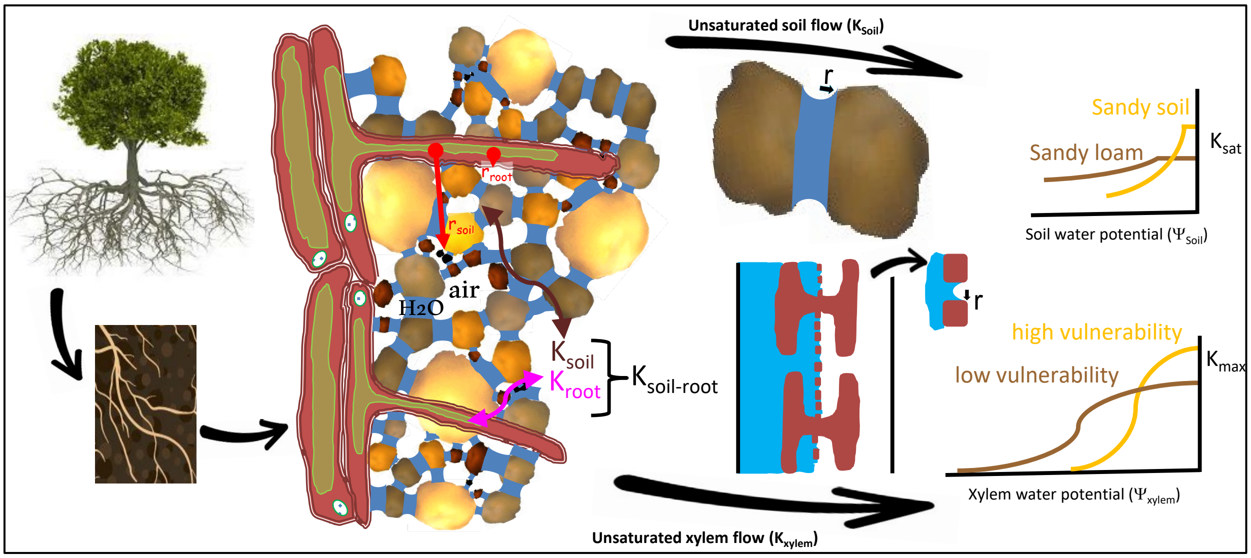

Figure 7: A conceptual representation of the contributions and the changes in soil (K_{soil}) and root hairs (K_{root}) hydraulic conductivity to rhizosphere conductance ($K_{soil\text{-}root}$). Water (blue) in soil is held by capillary forces in pore space (radius r) under negative pressure. As soil dries, soil water potential (Ψ_{soil}) becomes more negative and air replaces the water-filled pore space. Consequently, soil conductivity at saturation (K_{sat}) declines rapidly with Ψ_{soil} dependently of soil texture, with sandy (porous soils) having higher K_{sat}, and being more sensitive to Ψ_{soil} than for example sandy loam. Similarly, water in root xylem is also held at the interface of inter-conduit pits by capillary forces and as xylem water potential (Ψ_{xylem}) decreases air-seeding occurs (Figure 1), leading to an embolized conduit whose hydraulic conductivity declines from its maximum or fully hydrated values (K_{max}). Roots with high vulnerability to embolism have generally higher K_{max}, but analogous to porous soils, are also more sensitive to negative Ψ_{xylem} than roots with low vulnerability because of larger pit membrane pores. r_{root} and r_{soil} are root radius and the radial distance from the center of the roots to the mean distance between roots, respectively.